



On the effect of crustal layering on ring-fault initiation and the formation of collapse calderas

H.S. Kinvig^{*}, A. Geyer, J. Gottsmann

Department of Earth Sciences, University of Bristol, Wills Memorial Building, Queen's Road, BS8 1RJ, Bristol, England, United Kingdom

ARTICLE INFO

Article history:

Received 20 February 2009

Accepted 21 July 2009

Available online 28 July 2009

Keywords:

ring-fault
numerical modelling
caldera collapse
crustal layering
stress field

ABSTRACT

Collapse calderas can be attributed to subsidence of the magma chamber roof along bounding sub-vertical normal faults (ring-faults) after a decompression of the magma chamber. It has previously been shown that for ring-faults to initiate, and thus facilitate collapse, the stress field both at the surface and around the magma chamber must satisfy specific critical conditions. Here, we present new numerical models that use a Finite Element Method to investigate the effects of crustal layering on local stress field distribution. Results are compared with existing criteria for ring-fault initiation. Different subsurface scenarios were simulated by varying the stiffness (Young's modulus) of layers placed above the magma chamber, and the host rock in which the chamber is seated. We consider depressurisation of a magma chamber, so as to simulate magma withdrawal. Results indicate that mechanical layering is a further first-order variable in the rare achievement of stress conditions required for ring-fault formation, and may be influential in facilitating or inhibiting caldera collapse. We show that for a given geometrical set-up, the magnitude and position of maximum tensional stress at the Earth's surface are influenced by the occurrence and relative distribution of mechanically stiff or soft lithologies above the magma chamber. For example, tensional stress at surface may be reduced by the presence of stiff layers (e.g. lavas), or increased by soft layers (e.g. pyroclastic units) compared to generic simulations using a homogeneous background medium. Overall we find that the presence of mechanically soft material promotes surface fracture initiation. In addition we suggest that the position of peak tensional stress at surface derived by the numerical models does not represent that related to the position of the bounding ring-fault, but is instead related to the position of initial tensional fractures appearing prior to the collapse faults.

© 2009 Elsevier B.V. All rights reserved.

1. Introduction

Collapse calderas are associated with some of the largest and most violent and destructive volcanic eruptions on Earth. They also possess links with valuable ore deposits (e.g. Lipman, 1992, 2000; Guillou-Frottier et al., 2000) and geothermal resources (e.g. Kavouridis et al., 1999; Goff, 2002). Despite their huge economic importance and destructive potential, there are still many aspects of their formation that are poorly understood. Significant contributions to the understanding of caldera mechanisms are offered by field studies (e.g. Bailey et al., 1976; Sparks et al., 1985; Heiken et al., 1990; Allen, 2001; Lindsay et al., 2001) and further supported and expanded by analogue experimental models (e.g. Komuro et al., 1984; Komuro, 1987; Martí et al., 1994; Acocella et al., 2000, 2001, 2004; Walter and Troll, 2001; Kennedy et al., 2004; Geyer et al., 2006), numerical simulation (e.g. Gudmundsson et al., 1997; Gudmundsson, 1998, 2007; Burov and Guillou-Frottier, 1999; Folch and Martí, 2004; Gray and Monaghan,

2004) and geophysical investigations (Aprea et al., 2002; Steck and Prothero, 1994). The interested reader is also referred to Martí et al. (2008) for a recent review of different strands of investigations relating to caldera volcanism. Most collapse calderas can be attributed to subsidence of the magma chamber roof along bounding sub-vertical normal faults (ring-faults) after a decompression of the magma chamber is induced by eruption (e.g. Williams, 1941; Druitt and Sparks, 1984; Lipman, 1997).

Most of the existing mathematical models focusing on the stress conditions leading to ring-fault formation have been carried out assuming a homogeneous and isotropic host rock (e.g. Gudmundsson et al., 1997; Gudmundsson, 1998; Folch and Martí, 2004). This is however accepted to be a poor approximation to a natural system, in which heterogeneities exist, with different rock units both above and hosting the magma chamber comprising different materials with different mechanical properties (Fig. 1). For example, composite volcanoes and rift zones are generally composed of layers of predominantly pyroclastic rocks and lava flows, which commonly have highly contrasting mechanical stiffnesses (and thus contrasting Young's moduli (E)). Laboratory and in-situ measurements indicate that pyroclastic layers tend to be soft, with E as low as 0.05–0.1 GPa, whereas

^{*} Corresponding author. Tel.: +44 7515826118.

E-mail addresses: h.kinvig@bristol.ac.uk (H.S. Kinvig), A.Geyer@bristol.ac.uk (A. Geyer), J.Gottsmann@bristol.ac.uk (J. Gottsmann).

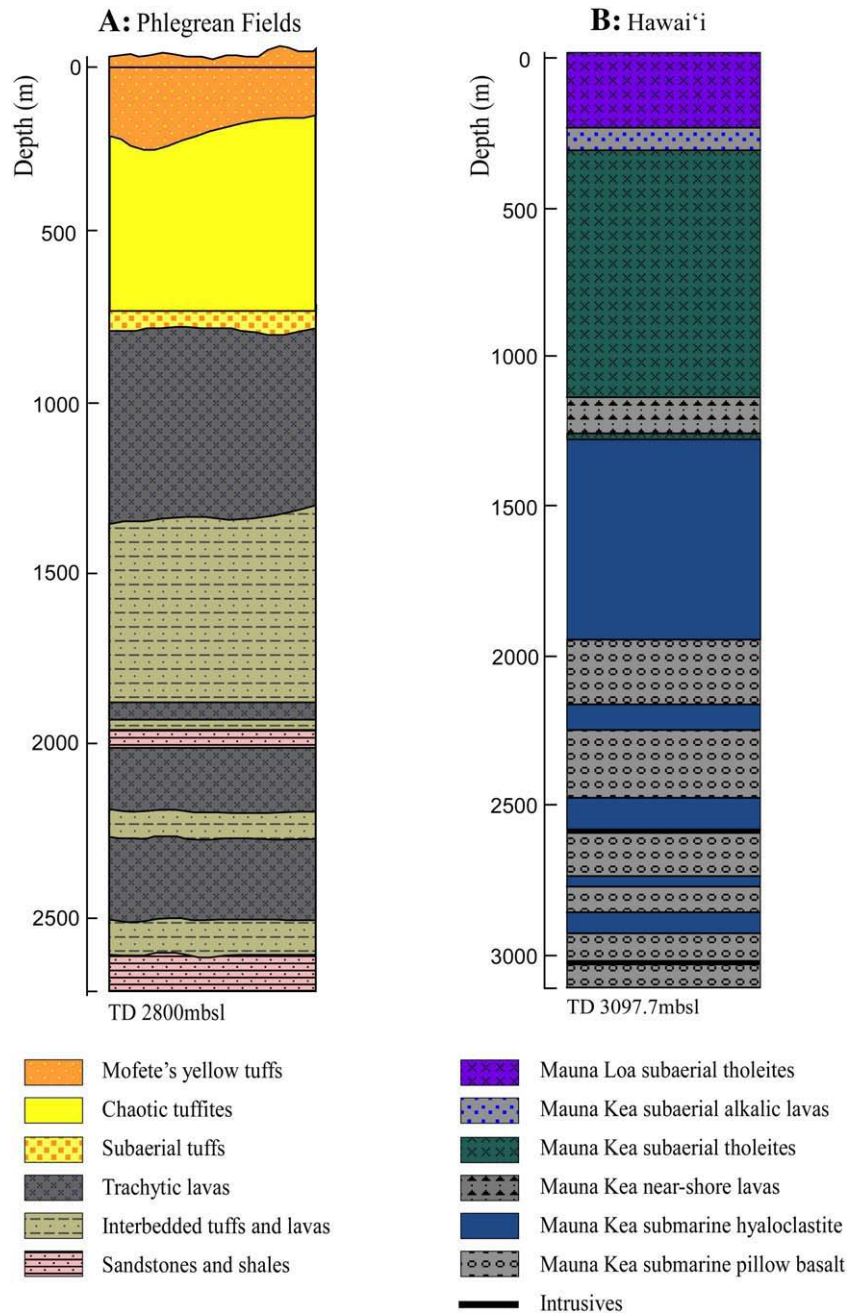


Fig. 1. A) Stratigraphic section of part of the Mofete area in the Phlegrean Caldera, Italy, illustrating the presence of alternating layers of mechanically stiff and soft units, including lavas and pyroclastic material. Subsurface data from geothermal well MF5. (Modified from *Rosi and Sbrana, 1987*). B) Stratigraphic section of part of Hawai'i volcano illustrating its make-up of predominantly mechanically stiff lavas. Subsurface data from Hawai'i Scientific Drilling Project core (HSDP2). (Modified from *Garcia et al., 2007*).

lava flows are normally stiff, with some basalts and gabbros having E as high as 110–130 GPa (Bell, 2000; Gudmundsson and Brenner, 2005; Gudmundsson and Philipp, 2006 and references therein). Such mechanical heterogeneities in crustal rocks can influence the distribution of stress concentrations around the magma chamber and consequently fracture propagation and ring-fault development (e.g. Gudmundsson and Brenner, 2005; Gudmundsson and Philipp, 2006; Gudmundsson, 2007).

In the present paper we investigate stresses in a layered crust above a shallow magma chamber subject to underpressure. The models are focused on investigating how the mechanical properties of subsurface strata (Young's modulus/density/thickness/order of layers) may affect stress field distributions (tensile and shear) and how these in turn affect the likelihood of ring-fault formation. Each mechanical layer is considered to be homogeneous and isotropic, whilst the model as a

whole can be considered anisotropic or transversely isotropic, as is typical of many layered rock bodies (e.g. Goodman, 1989; Hudson and Harrison, 1997). For simplicity, the models simulate horizontal layering and flat surface topography, although it is recognised that calderas often form in regions of significant topographic relief with dipping and/or folded strata making up the volcanic edifice. Our goal is to find out which mechanical configurations favour the stress-field conditions required for the initiation of ring-fault formation, and therefore caldera collapse.

2. Procedure

2.1. Geometrical setting and boundary conditions

To test the proposal that subsurface layering influences local stresses and therefore the generation of ring-faults, several numerical

runs with varying layered set-ups were made. Results were obtained using FEMFES, a code that solves elasticity problems using a Finite Element Method with nodal implementation (Codina and Folch, 2004).

The computational domain corresponds to an idealized cross-section of the upper crust which extends to a depth of 25 km below a flat surface and a lateral distance of 25 km (Fig. 2A). The sides and the bottom of each of the models are normal and parallel, respectively, to the top surface and are assigned as the arbitrary limits of the computational domain. We assume that during caldera collapse the surrounding crust behaves as a linearly homogeneous elastic material, within which an oblate magma chamber is modeled as a cavity. The magma chamber has a horizontal semi-axis a (horizontal extension $2a$) and vertical semi-axis b (vertical extension $2b$), and is located at depth d below the Earth's surface. For simplicity we assume axial symmetry, so that the orthogonal projection of the chamber at surface is a circle of radius a . The lateral and bottom computational margins are fixed so as to prescribe zero displacement, and the upper planar (Earth's) surface is a free surface (i.e. traction free). The decompressing magma chamber is represented by imposing a uniform radial underpressure ($-\Delta P$) of -15 MPa at the chamber walls, so as to simulate magma withdrawal. We chose this value to represent chamber underpressurisation deemed realistic to induce caldera formation as deduced by other investigations (e.g. Folch and Marti, 2004; Marti et al., 2000; Stix and Kobayashi, 2008; Geyer and Marti, 2009).

To simulate crustal layering seven layers of thickness t , where $t = d/10$, were placed above the magma chamber. The top of the uppermost layer is placed at a depth of $2t$, and a distance of t is also maintained between the bottom layer and the top of the magma chamber (Fig. 2B). Different stratigraphic set-ups were created by changing the mechanical properties (Young's modulus E , and density ρ) of the seven thinner beds above the magma chamber, and the remaining host rock, with each being given a value of $E = 18$ GPa and $\rho = 2200$ kg m $^{-3}$ (soft), $E = 45$ GPa and $\rho = 2500$ kg m $^{-3}$ (background value) or $E = 72$ GPa and $\rho = 2800$ kg m $^{-3}$ (stiff). Poisson's coefficient (ν) is kept constant, as it has been shown to have very little influence on results, and for all units $\nu = 0.25$, representing a typical Poisson's ratio for both basalts and soft pyroclastic rocks (Bell, 2000).

The property values (E, ρ, ν) were chosen such as to be representative of contrasting mechanical stiffness while also being geologically plausible in order to obtain general constraints of the influence of crustal layering on ring fault initiation, rather than to study the influence of particular rock types in detail. However, the soft layers can be considered representative of pyroclastic or sedimentary deposits, the stiff layers representative of lava flows, and the background value of $E = 45$ GPa represents average crustal values at a few kilometres depth (Gudmundsson, 2006).

We assume that the initial stress field surrounding the magma chamber is purely lithostatic with $\sigma_1 = \sigma_2 = \sigma_3 = \rho g z$, where σ_i ($i = 1, 2$, and 3) stands for the principal stresses, ρ is the mean density of the surrounding crust, z is depth from the Earth's surface and g is the gravitational acceleration ($g = 9.81$ m s $^{-2}$). The Earth's surface is here considered to be flat with no additional loading forces, so $\sigma_1 + \sigma_2 + \sigma_3 = 0$. It is important to note that the presence of topography, such as a volcanic edifice, would modify the stress distribution at surface affecting the conditions for caldera collapse (Pinel and Jaupart, 2005) and also the collapse symmetry, as shown by analogue models (Lavallée et al., 2004). The models also do not consider the influence of any pre-collapse fracturing or external regional tectonic stresses.

2.2. Stress field conditions for sub-vertical ring-fault formation

Numerical experiments have shown that for sub-vertical normal ring-faults to initiate, and so allow caldera collapse, the stress field around the magma chamber must satisfy three conditions simultaneously (Gudmundsson et al., 1997; Gudmundsson, 1998; Folch and Marti, 2004; Gudmundsson, 2007). These are: [C1] The minimum value of compressive stress (σ_3), that is the maximum tension, must occur at the Earth's surface, [C2] The maximum value of shear stress ($\sigma_1 - \sigma_3$) must occur at the lateral margins of the magma chamber, and [C3] The maximum tension (minimum σ_3) at surface, must peak approximately above the lateral ends of the magma chamber. Folch and Marti (2004) further constrained this latter condition to be verified only when the minimum value of σ_3 peaks at a radial distance from the centre of the magma chamber, between $a - h_{\max}$ and $a + h_{\max}$, where $h_{\max} = d \times \tan(\theta_{\text{crit}})$, and θ_{crit} is a critical angle in the range

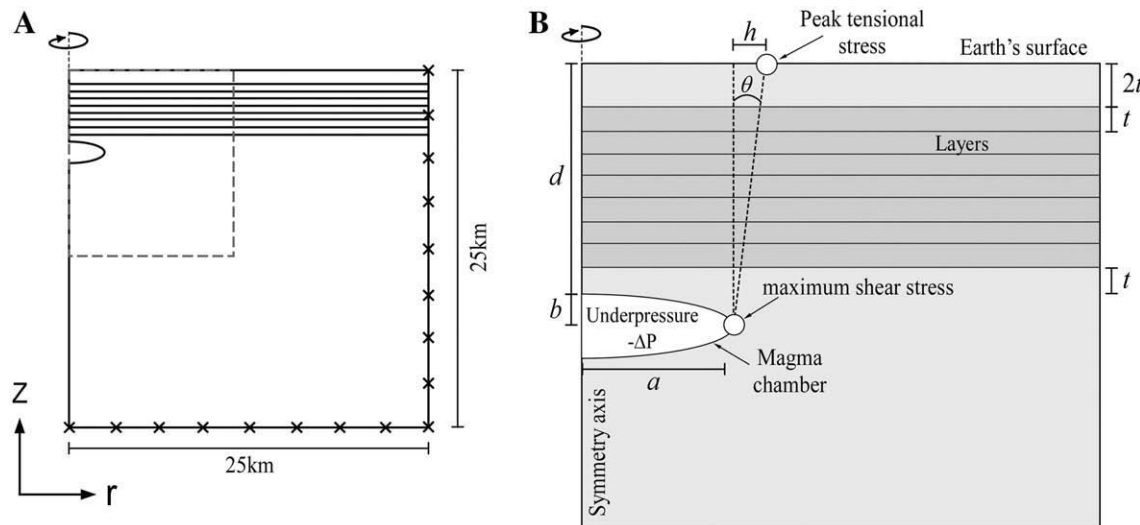


Fig. 2. A) Sketch of the computational domain showing the magma chamber. Boundary conditions have been illustrated, too. The models are axi-symmetric with rotation around the z -axis as indicated, so that the orthogonal projection of the chamber at surface is a circle of radius a . The magma chamber has an underpressure ΔP of -15 MPa imposed at the chamber walls. The Earth's surface is treated as a free surface (i.e. traction free) and the computational margins are fixed (i.e. zero displacement). Additionally, displacement in the r -direction is fixed to zero along the axis of symmetry (z). The broken box in A) indicates that part of the model shown in B) and in subsequent figures 6–12. B) An oblate magma chamber with axis a (horizontal extension $2a$), and b (vertical extension $2b$) is placed at depth d below the Earth's surface. Seven layers of thickness t (where $t = d/10$) are placed at depth $2t$ below the Earth's surface. The magma chamber is subjected to under-pressure ΔP of -15 MPa, simulating decompression. As discussed in Section 2.2., the formation of sub-vertical normal ring-faults is encouraged if critical conditions [C1] to [C3] are simultaneously satisfied; that is when [C1] the absolute minimum of σ_3 is at the surface, [C2] the maximum shear stress concentrates at the margins of the magma chamber (as indicated in B), and [C3] the peak of minimum σ_3 occurs at a radial distance between $a - h_{\max}$ and $a + h_{\max}$ where $h_{\max} = d \times \tan(\theta_{\text{crit}})$. (Figure modified after Folch and Marti (2004)).

or lower than 10–15°, between the vertical and the line drawn from the magma chamber edge to the surface peak of minimum σ_3 (Fig. 2B).

Gudmundsson (1988a,b) and Folch and Marti (2004) additionally showed that the formation of ring-faults is governed by the shape/depth configuration of the magma chamber, which can be parameterised defining the dimensionless parameters (1) $e = a/b$ and (2) $\lambda = a/d$. This second shape/depth configuration can be alternatively considered as the roof aspect ratio of the magma chamber $R = d/2a$, which is a measure of the thickness to width ratio of the chamber roof (Roche et al., 2000; Geyer et al., 2006; Scandone and Acocella, 2007).

2.3. Numerical method

To verify that the observed changes in stress distribution can be attributed to changes in the mechanical properties of the subsurface layers, rather than being due to changes in the model's geometry, two sets of numerical models were run with different R values maintained for each by changing either a (magma chamber horizontal extension) or d (magma chamber depth). This is in accordance with the observation of Folch and Marti (2004) that the (R, e) pair determines the collapse regime and that there is a critical combination of (R, e) that allows conditions [C1] to [C3] to be met, and thus initiate ring-fault formation. The first set of models kept the size of the magma chamber constant ($a = 2500$ m, $b = 750$ m) and changed its depth from $d = 1000$ m–5000 m deep, giving R values of 0.2–1, respectively. The thickness of the overlying subsurface layers were also kept relative to the depth of the magma chamber so that $t = d/10$. Magma chambers with $R < 1$ were chosen as previous studies indicate that such aspect ratios develop coherent piston-type collapse, whereas higher roof aspect ratios (e.g. $R \geq 1$: Roche et al., 2000; $R \geq 0.7$ –0.85: Geyer et al., 2006; $R \geq 1.6$: Scandone and Acocella, 2007) form incoherent collapse. The second set of models kept depth constant at $d = 5000$ m and maintained the same set of R values used in the first set of models by changing the length of a accordingly, thus changing the ellipticity (e) of the chamber. Only oblate (sill-like) chambers were modelled ($e < 1$), since prolate ($e > 1$) chambers have been proposed to be unlikely to form ring-faults (e.g. Gudmundsson, 1988a,b, 2007; Gudmundsson et al., 1997; Folch and Marti, 2004).

3. Results

Several numerical models were run with different stratigraphic set-ups generated by varying the mechanical properties (Young's modulus and density) of each of the thin crustal layers above the magma chamber. A homogenous setting, whereby the seven layers and the remaining host rock share the same mechanical properties, was also modelled as a reference against which to compare the other models. Only relevant results are exposed here.

We ran several different geometrical set-ups varying R , to confirm that the changes in stress distribution observed are due to the variations in layering in each of the models, and not the result of a shape/depth configuration control. We observed that decreasing R increased the tensional stress (σ_3) at surface, and resulted in a much more focused distribution of stress, with peak tensile stress (σ_3) occurring closer to the surface-projection of the edge of the magma chamber and the critical distance dictated in [C3]. Conversely, magma chambers with higher R values produced lower tensional stress at the surface, further from the critical distance necessary to initiate ring-faults (Fig. 3). These results are in agreement with previous observations (e.g. Folch and Marti, 2004).

In all our models the maximum tensional stress (σ_3) occurs at the Earth's surface, thus satisfying critical condition [C1] (Fig. 4A) and the maximum shear stress ($\sigma_1 - \sigma_3$) occurs at the lateral margins of the magma chamber, thus satisfying condition [C2] (Fig. 4B). In addition, in all our models the surface expression of tensional stress (σ_3) forms a peak above the projected edge of the magma chamber,

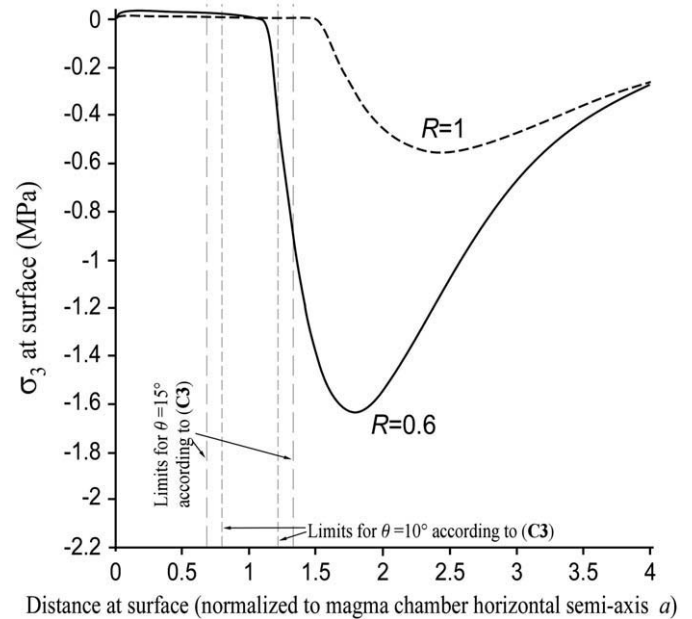


Fig. 3. Principle tensile stress (σ_3) at the Earth's surface plotted against radial distance from the centre of the magma chamber, for models with a homogeneous host rock and roof aspect ratio $R = 0.6$ and $R = 1$. Radial distance is normalised to chamber extension, i.e. the surface projection of the magma chamber margins occurs at dimensionless distance 1. The origin of coordinates is at the symmetry axis. For both models $a = 2500$ m and $b = 750$ m. For $R = 0.6$ the magma chamber is located at depth $d = 3000$ m, for $R = 1$ the magma chamber is located at depth $d = 5000$ m. The critical distances defined by condition [C3] for $\theta = 10^\circ$ and $\theta = 15^\circ$ are marked with dashed vertical lines in this figure and all subsequent figures. Note how for the lower roof aspect ratio ($R = 0.6$) the peak of minimum σ_3 is greater, more focused and occurs closer to the edge of the magma chamber. Neither scenario generates a peak of tensile stress within the critical distances defined by condition [C3].

however in most models these peaks lie outside the critical distance defined by $a - h_{\max}$ and $a + h_{\max}$ (Folch and Marti, 2004), unless they have a very low R value, representing unrealistic depth or width arrangements (either too shallow or too wide compared to what is seen in nature). Thus there is a geometrical control on satisfaction of condition [C3].

3.1. Homogeneous model

For the homogeneous models, the seven thin layers and remaining host rock share the same mechanical properties. For a given shape/depth configuration, the magnitude and distribution of tensional stress at surface remains constant, regardless of the mechanical properties of the host unit. This suggests that the surface variations in tensile stress (σ_3) observed in the following heterogeneous models (Section 3.2) are a direct result of the presence of layering, specifically the mechanical contrast between layers.

3.2. Heterogeneous models

3.2.1. Influence of changing the thickness of a stiff or soft layer

Models were generated to look at the effect of increasing the thickness of a stiff (72 GPa) or soft (18 GPa) layer placed near the surface, while a background value of 45 GPa comprises the remaining layers and host rock. The tensional stress (σ_3) recorded at the Earth's surface for a stiff or soft layer of thickness $5t$ and $7t$ is shown in Fig. 5. The results reveal that the addition of a stiff layer will decrease the magnitude of tensional stress recorded at surface, and this stress is further reduced by increasing the thickness of the stiff layer. The opposite effect is observed for the addition of soft layers, with a thicker soft layer giving the greatest tensional stress at surface. The difference

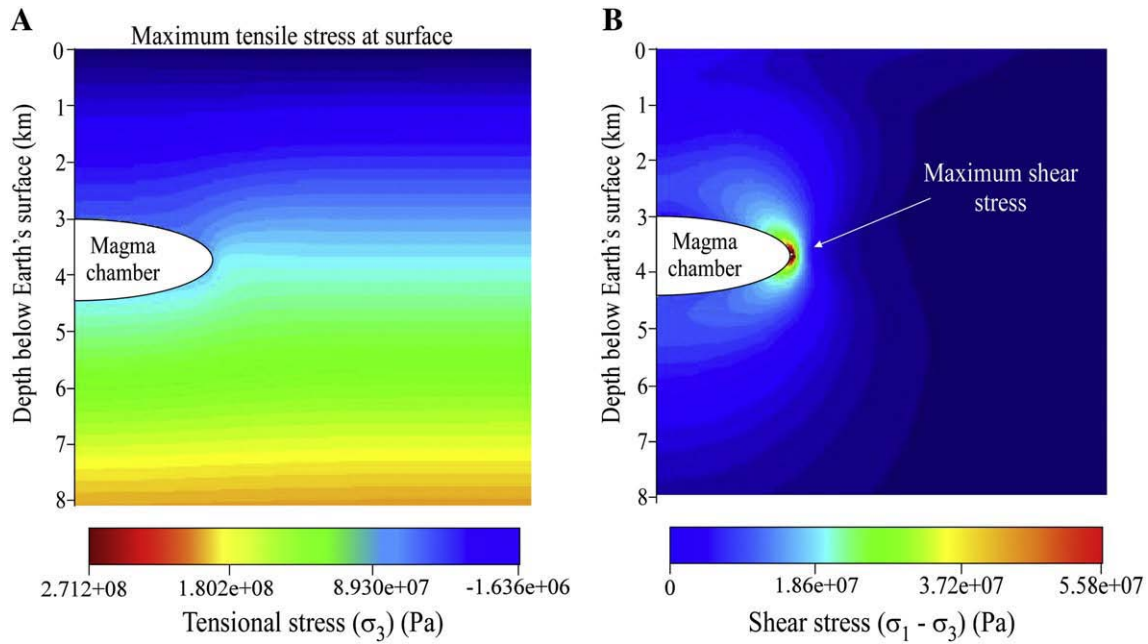


Fig. 4. Contours illustrating stress field distributions around a magma chamber with $a=2500$ m, $b=750$ m, and $d=3000$ m, so $R=0.6$, after a magmatic decompression of -15 MPa. The magma chamber was located in a homogeneous, isotropic host rock. Only the region of the computational domain around the magma chamber is shown. Stresses are given in Pa. A) Contours of tensile stress (σ_3) (lithostatic plus syn-eruptive variations), illustrating that condition [C1] here holds true, with the maximum tensile stress occurring at the Earth's surface. B) Contours of shear stress ($\sigma_1 - \sigma_3$), illustrating that condition [C2] here holds true, with the maximum shear stress occurring at the lateral margins of the magma chamber.

in magnitude of σ_3 is less influenced by changing the thickness of a stiff layer, and is more pronounced with increasing numbers of soft layers.

Thickening a stiff layer also has the effect of moving the peak of maximum tension (minimum σ_3) further from the edge of the magma chamber, and therefore further from the critical distance in which it would need to occur in order to satisfy condition [C3] according to

Folch and Marti (2004), and conversely thickening a soft layer will move the peak of maximum tension closer to the edge of the magma chamber (Fig. 5). Though only slight, this shift in peak tensile stress towards or away from the magma chamber edge becomes more noticeable with increasing R (i.e. deeper magma chambers or those with less horizontal extension).

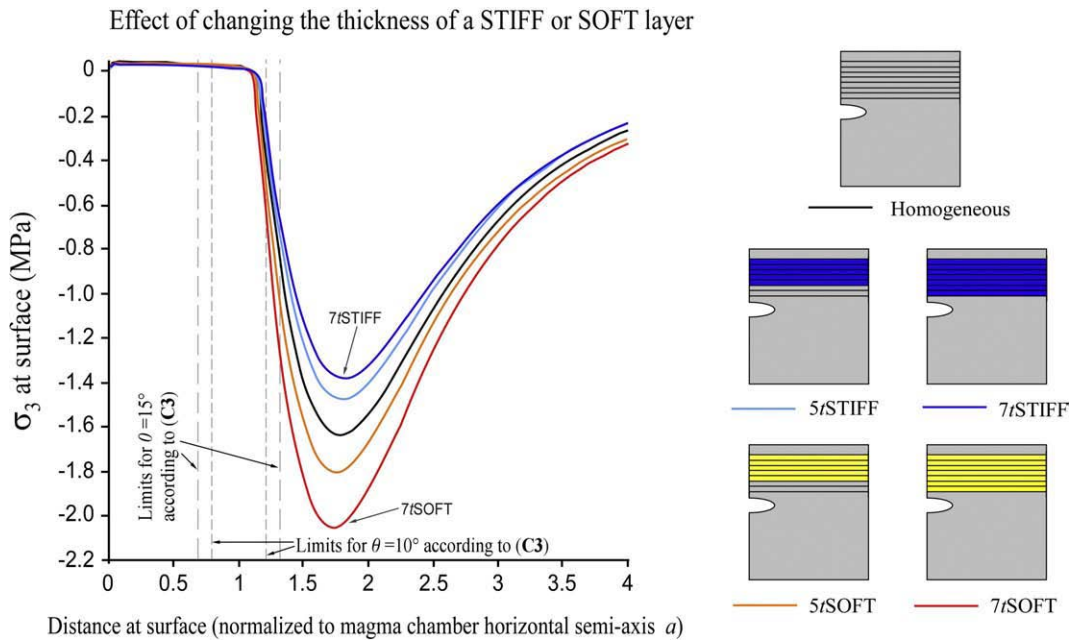


Fig. 5. Left: Principle tensile stress (σ_3) at the Earth's surface plotted against radial distance from the centre of the magma chamber to show the effect of changing the thickness of a STIFF ($E=72$ GPa) or SOFT ($E=18$ GPa) layer above the magma chamber. Values for a homogeneous host rock, of stiffness $E=45$ GPa, are also plotted with a bold line for comparison. Magma chamber with $a=2500$ m, $b=750$ m, and $d=3000$ m, so $R=0.6$, after a magmatic decompression of -15 MPa. Radial distance is normalised to chamber extension, i.e. the surface projection of the magma chamber margins occurs at dimensionless distance 1. The origin of coordinates is at the symmetry axis. The critical distances defined by condition [C3] for $\theta=10^\circ$ and $\theta=15^\circ$ are marked with dashed vertical lines. Right: Images depicting the different layering scenarios plotted. Note that increasing the thickness of a STIFF layer decreases tensile stress at surface, and moves the peak of σ_3 further from the magma chamber edge, while increasing the thickness of a SOFT layer increases tensile stress and moves the peak of σ_3 closer to the edge of the magma chamber.

3.2.2. Changing the proportion of STIFF:SOFT layers and their vertical order

The mechanical properties of the seven thin crustal layers were then varied so as to generate ratios of 3t:4t and 4t:3t for 72 GPa:18 GPa and 18 GPa:72 GPa, with 45 GPa comprising the remaining host rock (Fig. 6). For both 72 GPa:18 GPa and 18 GPa:72 GPa ratios, increasing the proportion (thickness) of soft layers results in greater tensional stress at the surface. The vertical order of the layers also influences the magnitude of tensional stress: having a soft layer beneath a stiff layer, or viewed alternatively as placing the soft layer closer to the top of the magma chamber, will generate greater tension at surface than the same thickness of soft material placed above a stiff layer.

It is also observed that for any given stiff:soft ratio with x -many stiff layers at the top, the resulting tensional stress at the surface is greater and peaks closer to the magma chamber edges, than models with the same number and position of stiff layers with all remaining units as 45 GPa. Similarly for any given soft:stiff ratio, the surface tension is lower and peaks further from the critical distance with the addition of stiff layers compared to a 45 GPa background. This suggests that in general the addition of softer units will generate a tensional stress field at surface that is more favourable to ring-fault initiation and therefore caldera collapse.

3.2.3. Changing the depth of a stiff or soft layer

A stiff or soft layer with thickness $3t$ was placed at varying depths in the subsurface, whilst maintaining a background stiffness of 45 GPa in all other units (Fig. 7). It was found that increasing the depth of a stiff layer, so as to place it closer to the top of the magma chamber, reduces the magnitude of tensional stress at the Earth's surface, whilst placing a soft layer at greater depths gives greater tension at the Earth's surface. Varying the depth of a soft layer is more influential in altering

the degree of tensional stress at surface than the placement of a stiff layer.

3.2.4. Changing the depth of a stiff or soft layer whilst a contrasting layer remains at the surface

Models were then run with either a stiff or soft layer of thickness $2t$ placed near the surface, whilst a $2t$ thick layer of contrasting stiffness was placed at varying depths below (Fig. 8). In all of these models the number and proportion of stiff and soft layers remains the same, with each comprising a total thickness of $2t$ in each model. All other layers and the remaining host rock were given a background value of 45 GPa. Regardless of the vertical order of layers (i.e. stiff above soft or soft above stiff) the deeper a layer is placed the greater the magnitude of tensional stress generated at the surface. However, changing the depth of a stiff layer below a soft layer (Fig. 8) makes very little difference to the magnitude of tensional stress at the surface, particularly when compared with the variation induced by deepening a soft layer below a stiff layer (Fig. 8). Furthermore, placing a soft layer below a stiff layer, regardless of the depth configuration, will produce greater tension at the Earth's surface compared with a homogeneous model, whilst conversely a stiff layer located below a soft layer will always generate less tension at the surface. This magnitude variation in peak stress is more apparent for magma chambers of greater ellipticity (increasing e). These observations therefore suggest that for a given proportion of stiff to soft layers, the order of layers is the key factor controlling the magnitude of tensional stress at the surface. The results concur with those models that change the ratio of stiff:soft layers (Section 3.2.2). It is also observed that the position of the peak tensional stress varies laterally with the different stratigraphic setups.

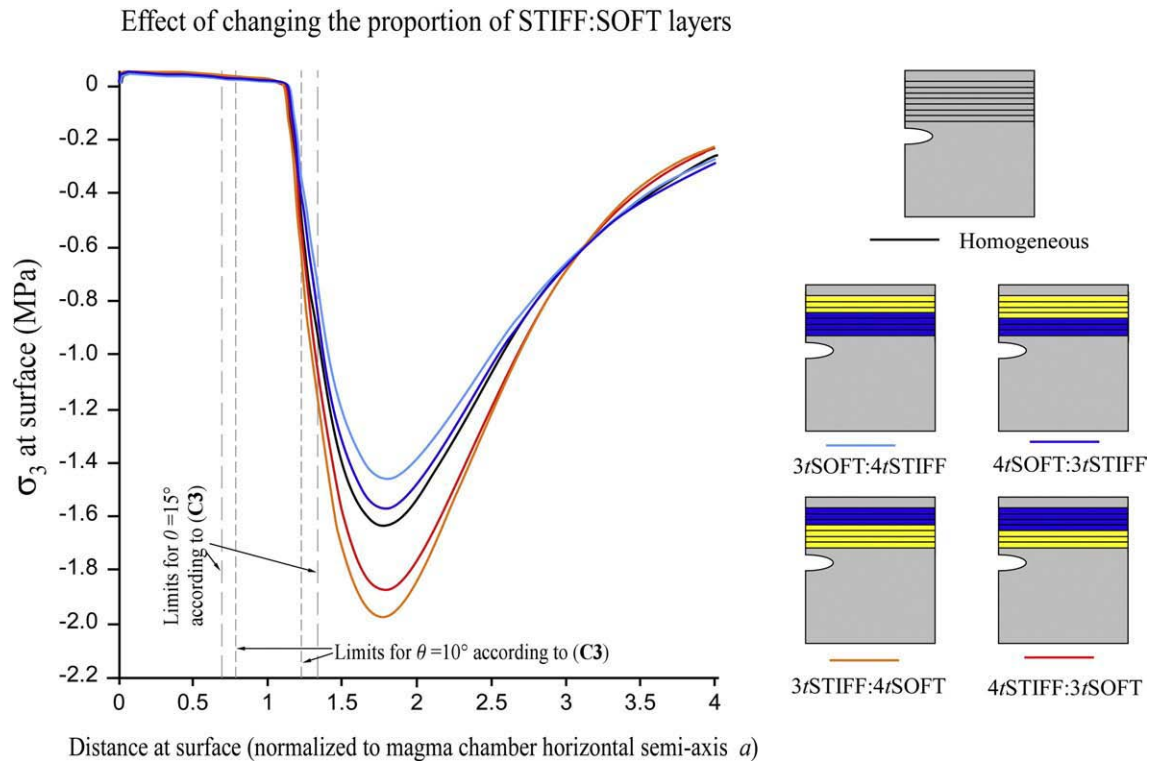


Fig. 6. Left: Principle tensile stress (σ_3) at the Earth's surface plotted against radial distance from the centre of the magma chamber to show the effect of changing the proportion of STIFF (72 GPa) to SOFT (18 GPa) layers above the magma chamber. Values for a homogeneous host rock, of stiffness 45 GPa, are also plotted with a bold line for comparison. Magma chamber with $a = 2500$ m, $b = 750$ m, and $d = 3000$ m, so $R = 0.6$, after a magmatic decompression of -15 MPa. Radial distance is normalised to chamber extension, i.e. the surface projection of the magma chamber margins occurs at dimensionless distance 1. The origin of coordinates is at the symmetry axis. The critical distances defined by condition [C3] for $\theta = 10^\circ$ and $\theta = 15^\circ$ are marked with dashed vertical lines. Right: Images depicting the different layering scenarios plotted. Note that increasing the proportion of STIFF layers decreases tensile stress at surface, while increasing the proportion of SOFT layer increases it. Placing a soft layer below a stiff layer will generate greater tensional stress at surface than a homogeneous host rock or a stiff layer placed below a soft layer.

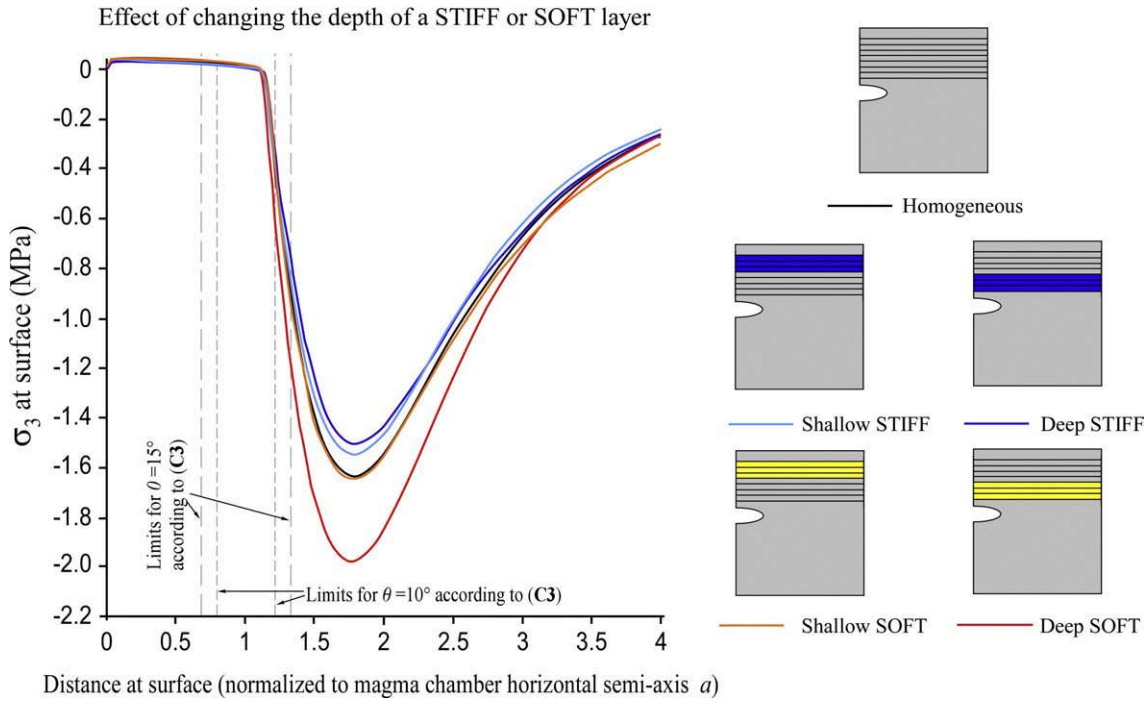


Fig. 7. Left: Principle tensile stress (σ_3) at the Earth's surface plotted against radial distance from the centre of the magma chamber to show the effect of changing the depth of a STIFF (72 GPa) or SOFT (18 GPa) layer above the magma chamber. Values for a homogeneous host rock, of stiffness 45 GPa, are also plotted with a bold line for comparison. Magma chamber with $a = 2500$ m, $b = 750$ m, and $d = 5000$ m, so $R = 1$, after a magmatic decompression of -15 MPa. Radial distance is normalised to chamber extension, i.e. the surface projection of the magma chamber margins occurs at dimensionless distance 1. The origin of coordinates is at the symmetry axis. The critical distances defined by condition [C3] for $\theta = 10^\circ$ and $\theta = 15^\circ$ are marked with dashed vertical lines. Right: Images depicting the different layering scenarios plotted. Note that increasing the depth of a STIFF layer decreases tensile stress at surface while increasing the depth of a SOFT layer increases tensile stress at surface.

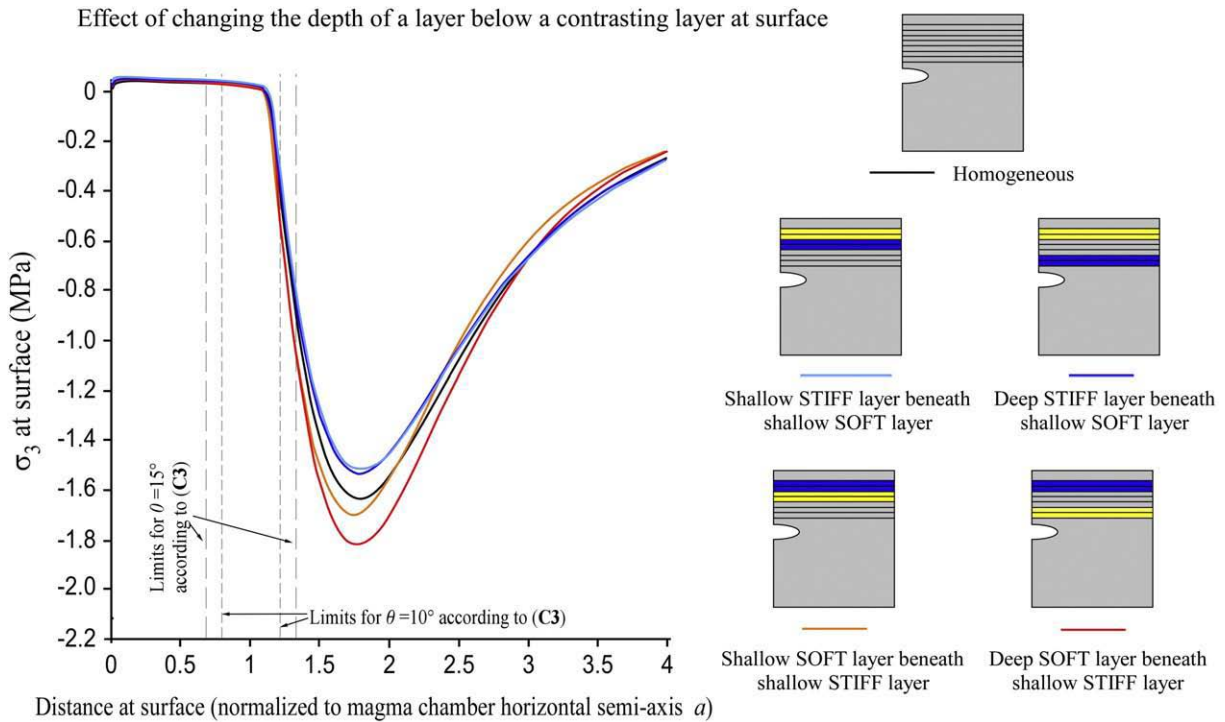


Fig. 8. Left: Principle tensile stress (σ_3) at the Earth's surface plotted against radial distance from the centre of the magma chamber to show the effect of changing the depth of a STIFF (72 GPa) or SOFT (18 GPa) layer below a shallow layer of contrasting stiffness. Values for a homogeneous host rock, of stiffness 45 GPa, are also plotted with a bold line for comparison. Magma chamber with $a = 2500$ m, $b = 750$ m, and $d = 5000$ m, so $R = 1$, after a magmatic decompression of -15 MPa. Radial distance is normalised to chamber extension, i.e. the surface projection of the magma chamber margins occurs at dimensionless distance 1. The origin of coordinates is at the symmetry axis. The critical distances defined by condition [C3] for $\theta = 10^\circ$ and $\theta = 15^\circ$ are marked with dashed vertical lines. Right: Images depicting the different layering scenarios plotted. Note that regardless of the vertical order of layers (i.e. stiff above soft or soft above stiff) the deeper a contrasting layer is placed the greater the magnitude of tensional stress generated at the surface. A soft layer below a stiff layer, regardless of the depth configuration, will produce greater tension at the Earth's surface compared with a homogeneous model. Conversely a stiff layer located below a soft layer will always generate less tension at the surface.

4. Discussion

4.1. Influence of layering on stress-field conditions and implications for ring-fault initiation

The results of the numerical models presented here indicate that varying the mechanical properties of crustal layers above a magma chamber influences the magnitude and distribution of tensional stress (σ_3) at the Earth's surface (Fig. 9). The occurrence and relative distribution of mechanically different lithologies may therefore be influential in generating or inhibiting caldera collapse in otherwise favourable or unfavourable geometric settings, by either encouraging or discouraging the stress conditions required for the initiation of ring-faults. It is only the initiation of these ring-faults at the Earth's surface that we focus on in this paper, and we do not consider the propagation of these faults between the magma chamber and the surface.

Overall it is shown that the presence and addition of mechanically soft layers will result in greater tensional stress at the Earth's surface

whilst the opposite is true for the occurrence of mechanically stiff layers (e.g. Fig. 5). This has important implications on the geological setting in which critical stress conditions for ring-fault initiation can be achieved. Volcanic terrains which include soft pyroclastic or sedimentary layers, such as is typical of intermediate-felsic volcanoes, are therefore more likely to generate the higher tensional stress conditions required to overcome the rock's tensional strength, and thus facilitate brittle failure and the opening of a surface fracture, than a mechanically stiff, e.g. lava dominated, environment. This is supported by field evidence, with over twice as many collapse calderas associated with composite strato-cones than for basaltic shields and lava domes/flows combined (Geyer and Martí, 2008).

Ongoing activity may then act to further affect a chamber's future collapse potential by depositing additional mechanically contrasting layers either at surface by eruption or at depth by intrusion. In this way a magma reservoir over time could achieve a more or less favourable configuration for ring-fault initiation and therefore collapse. A volcanic terrain that produces predominantly unconsolidated tephra

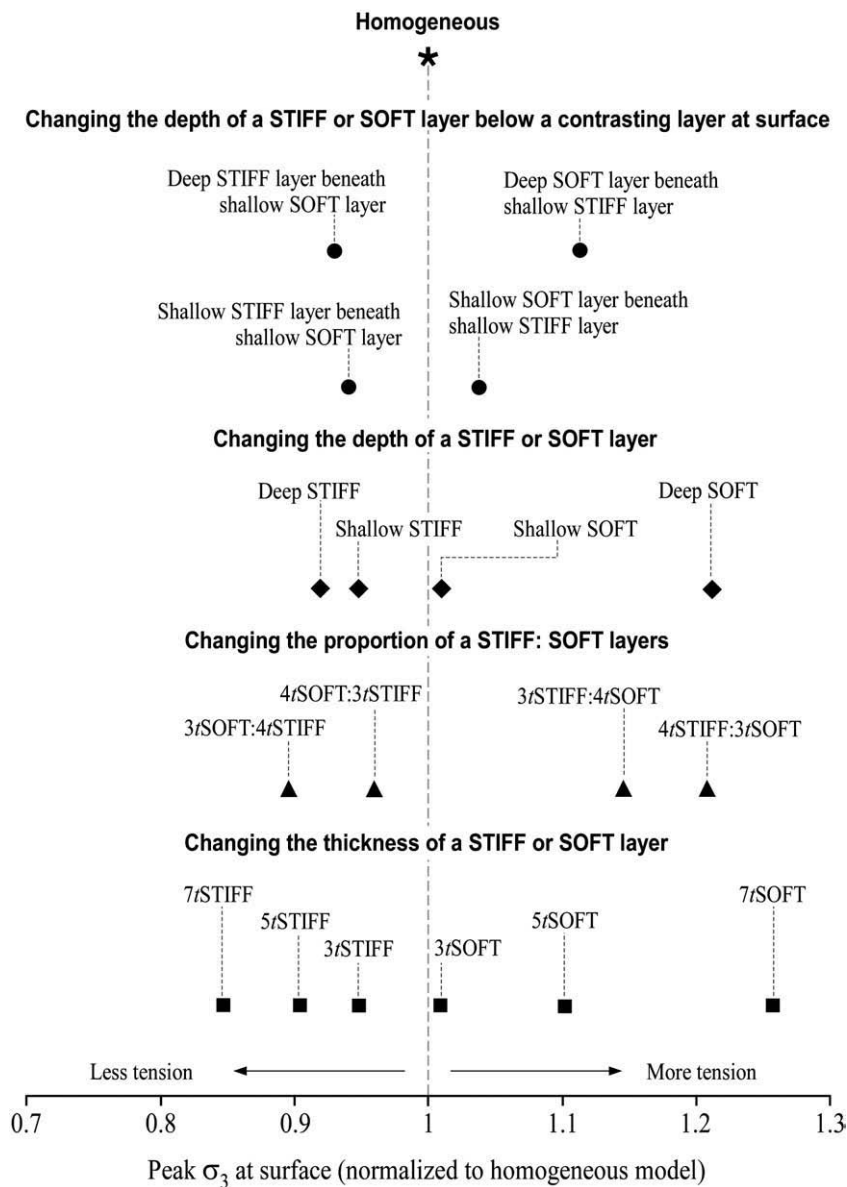


Fig. 9. Plot of maximum tensile stress (minimum σ_3) recorded at surface for each of the layering scenarios modelled. Stress values are normalised to those recorded for a homogeneous host rock, to illustrate the effect of layering. Those models plotted to the right of the homogeneous results (values >1) generate greater tension at surface, and those on the left (values <1) generate less tension at surface. In general those models generating less tension are those with STIFF layers present, and those generating more tension include SOFT layers.

and pyroclastic flow deposits will be increasing the thickness and proportion of mechanically soft layers above the magma chamber and therefore generating a configuration that is more propitious for the stress conditions required to initiate fractures at surface. Conversely the eruption of lava flows or domes could act to stiffen up the volcanic edifice, thus reducing the likelihood of the volcano reaching critical stress conditions and making it more difficult to generate a ring-fault. Similarly the intrusion of dykes and sills will add mechanical stiffness at depth, which has been shown here to decrease the magnitude of tensional stress at the surface (Fig. 7).

Evidence for this could be taken from chambers that fed multiple large explosive eruptions before eventually under-going a caldera-collapse during a climatic stage. Likewise, despite the eruption of a considerable volume of magma, caldera formation may be hindered if a reservoir has been predominantly feeding the emplacement of mechanically stiff material or is embedded in mature crust without longstanding volcanism and significant deposition of mechanically soft volcanic rocks. The 1600 AD non-caldera forming eruption of 12 km³ (DRE) of dacite magma at Volcán Huaynaputina would fit the latter criteria (Lavallée et al., 2006), whereas conditions for caldera formation might have been more favourable during the evolution of the Southern Rocky Mountain volcanic field (Lipman, 2007).

The relative order of lithologies is also shown here to be important in the transfer of tensional stress to the Earth's surface. A soft layer located below a mechanically stiffer layer will generate greater tensional stress at the Earth's surface than the opposite scenario (Figs. 6 and 8). In this way even if lavas were erupted so as to increase the proportion of mechanically stiff material above the magma chamber, if a sequence of soft, e.g. pyroclastic, material exits between it and the magma chamber, the tensional stress at surface could still be favourable to the conditions required for ring-fault initiation. This concept would also apply to the addition of soft pyroclastic material at surface above stiff lava, whereby the same relative proportions of stiff:soft material may exist as with the previous example, but the tensional stress at surface will be lower by virtue of the stiff material occurring deeper and so closer to the top of the magma chamber. In both circumstances, the greater the vertical distance between mechanically contrasting layers the greater the tensional stress appears to be at the surface. This observation is most significant for the deep intrusion of stiff sills below soft layers at surface.

It appears that knowledge of the pre-caldera subsurface lithology could prove crucial in understanding caldera collapse, particularly if wishing to forecast future collapse potential from current or ongoing activity. Such information may be obtained from borehole data or field observations. For example, from our results, of the two stratigraphic columns shown in Fig. 1, the Phlegrean Fields (log 1A) would likely generate greater tensional stress at the surface than the sequences displayed for Hawaii i (log 1B) due to the presence of soft tuff layers. The Hawaiian stratigraphic column is composed entirely of stiff lavas and so would generate lower magnitudes of tensional stress at the surface, thus reducing the likelihood of fracture initiation at the surface.

It must be noted here that the propagation of ring-faults is not investigated in this paper. We are not assessing whether a particular lithological configuration will or will not undergo caldera collapse, but instead investigate how different mechanical arrangements could favour or inhibit the stress conditions required for tensional failure to occur, and thus facilitate the formation of ring-faults at the surface.

Gudmundsson (2006, 2007) discusses the need for stress-field homogenisation, i.e. the alignment of stresses between layers so as to allow the trajectory of failure to continue without arrest, for a fault to successfully propagate between the magma chamber and the Earth's surface. Such stress-field homogenisation is more likely to be achieved through layers of similar mechanical properties, and for this reason he proposes that ring-faults and subsequent caldera collapse are more likely to occur in volcanic edifices composed of similar rather than contrasting materials, with a greater frequency of collapse events in basaltic shields compared with composite edifices. While the concept

that for fault-tip propagation to occur the most encouraging situation would be one in which the edifice is composed of similar mechanical properties (e.g. Gudmundsson, 2009) is not under dispute, the results of this current paper do however suggest that the initiation of a fracture (e.g. ring-fault) at surface is likely more achievable in an edifice composed of contrasting mechanical layers, particularly those comprising soft layers such as a composite volcano, due to the higher magnitude of tensional stress expressed at the surface. Furthermore, these frequencies are backed up in nature with most calderas associated with strato-volcanoes (Geyer and Martí, 2008).

Mechanically contrasting layers may also dramatically change the attitude of a fault as it propagates through differing lithologies due to elastic mismatch favouring fracture deflection, and this may be important in the overall attitude of the generation of a normal-type ring-fault. However, the results of our models additionally show that overall the position of fracture initiation at the surface changes very little even for greatly varying stratigraphic configurations. There does however appear to be a greater lateral shift in the position of peak tensional stress for magma chambers with higher roof aspect ratios. Numerical models of homogeneous settings have previously shown that magma chambers with either higher roof aspect ratios (R) or less oblate geometries (low e) are less likely to form peak tensional surface stress within the critical distance for ring-fault initiation in [C3] (Folch and Martí, 2004; Gudmundsson, 2007). This lateral shift induced by different stratigraphic properties could therefore prove influential in generating or inhibiting caldera collapse in otherwise unfavourable geometric conditions.

4.2. Considerations regarding local stress field conditions for ring fault initiation

Previous studies have proposed that for a collapse caldera controlling ring fault to initiate, the local stress field around the magmatic system must simultaneously satisfy three specific criteria (conditions C1–C3) as described in Section 2.2. Several published investigations into which geometrical configurations are required in order to generate this 'ideal' stress field propitious to ring-fault formation, by deflation of the magma chamber, have shown that to achieve this proper stress state is not trivial and only a few restricted geometric configurations may be potential caldera-forming systems. In particular, it is condition [C3] that is the most difficult to satisfy.

As we can observe here from our own results, the stress field related to the geometrical and stratigraphic configuration used exhibits maximum tensional stress at the surface (Fig. 4A) and maximum shear stress around the magma chamber margins (Fig. 4B), thus meeting critical conditions for ring-fault formation [C1] and [C2]. Furthermore, the tensional stress exceeds the tensional strength (T_0) of the host rock and so overcomes the Griffith failure criteria ($\sigma_3 \leq -T_0$) and therefore facilitates the production of tensional fractures at the Earth's surface. Likewise the shear stress around the magma chamber exceeds the shear strength (S_0) of the host rock and so facilitates shear failure at the magma chamber boundaries, by overcoming the Mohr–Coulomb shear failure criteria ($\sigma_1 - \sigma_3 \geq S_0$). However, none of the models meet condition [C3]. Even with the most advantageous stratigraphic set-up the position of maximum tensional stress at surface does not occur within the critical distance, defined as between $a - h_{\max}$ and $a + h_{\max}$ by Folch and Martí (2004), despite the magma chambers used here having realistic dimensions and depths ($R = 0.6$, $e = 3.33$, $a = 2.5$ km, $d = 3$ km). Only models with very low R and high e values, will produce a peak in tensile stress inside this critical distance range. There is therefore a definite geometrical control on satisfaction of condition [C3] and one that is clearly not consistently met in nature. Available data (e.g. Geyer et al., 2006; Geyer and Martí, 2008) show that not all caldera systems strictly fit these geometrical conditions (e.g. Ceboruco, Jala Pumice, Browne and Gardner, 2004; Vesuvius, Pompeii Pumice, Macedonio et al., 1994) and yet still achieve ring-fault formation

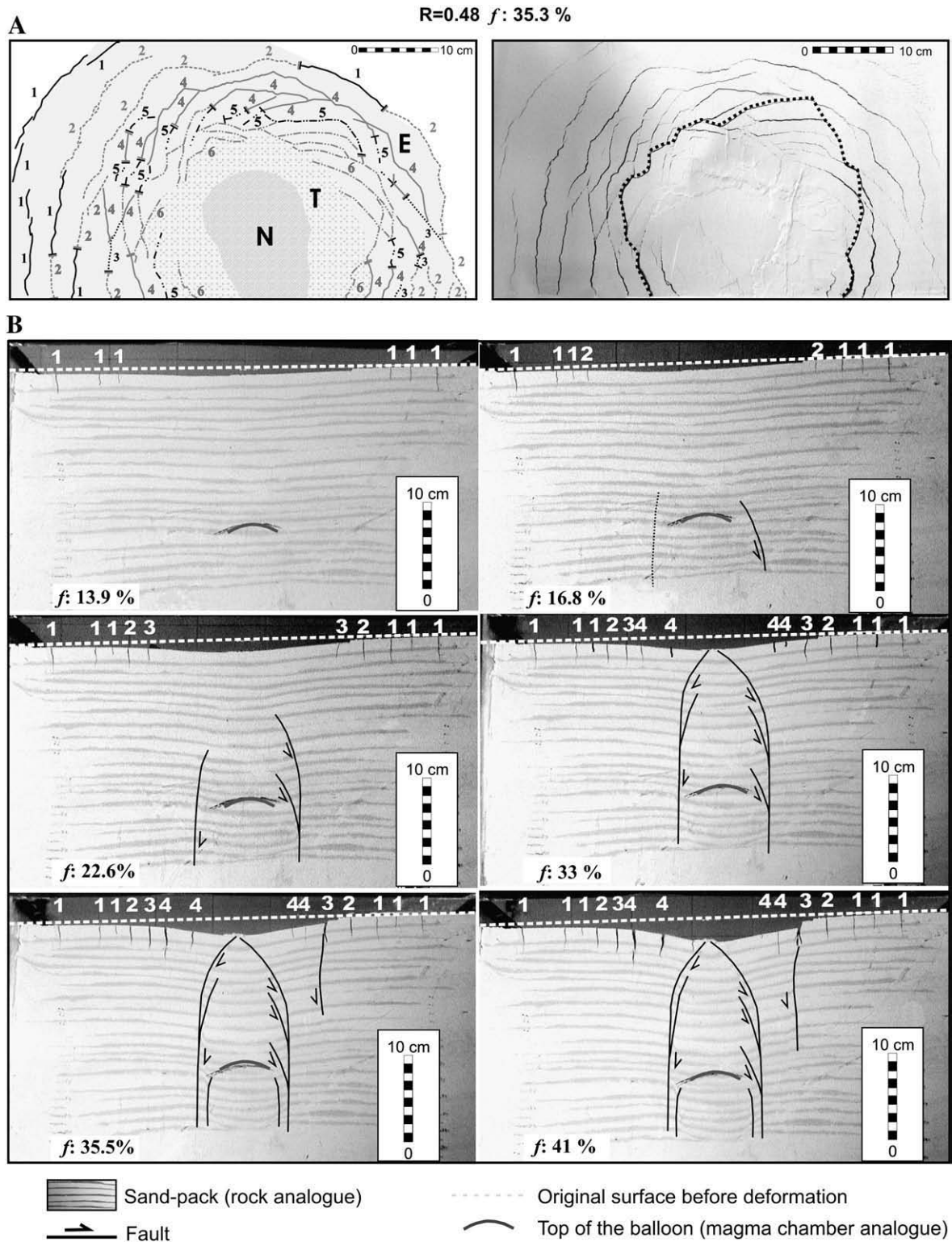


Fig. 10. Results obtained with experiment E-5 of Geyer et al., 2006. The experiment uses dry quartz sand and a water-filled latex balloon as host rock and magma chamber analogue, respectively. White and coloured layers of analogue material with equal physical properties stripe at regular depth intervals. The balloon is buried at a lateral wall of the box and has a tube connected to it. The unblocking of the tube allows water to flow out inducing a gradual deflation of the balloon that leads to the collapse of the overlying structure. The temporal evolution of the phenomenon is recorded by a video camera (see Fig. 1, Geyer et al., 2006 for more details). A) Scheme of surface fractures inferred from photographs. Numbers indicate the order of appearance of the corresponding fracture segment. Plane view observations allow us to define two different regions at surface: a non-deformed central area (N) and an annular zone of flexure and extension encircling the former. This external region can be subdivided, in turn, into a zone where strata are tilted towards the depression (T) and a horizontal area with extensive surface fractures (E). Surface fractures are clearly visible at the extensional zone. Black broken lines indicate the fractures that will evolve into vertical or sub-vertical ring faults and will delimit the piston subsidence during the last stages. (Modified from Geyer et al. (2006).) B). Different shots of the caldera collapse process. Additionally, the removed volume fraction f (volume of extruded magma/total volume of the magma chamber) is indicated in each photograph. White numbers, in concordance with those of Fig. 2, indicate the order of appearance of fractures at surface. (Modified from Geyer et al. (2006).)

facilitating collapse. From this apparent contradiction we infer that the results from numerical models may have been misinterpreted.

Analogue experiments of evacuating magma chambers record superficial tensional fractures occurring just at the beginning of the subsidence processes and far away from the central collapse area (e.g. Geyer et al., 2006) (Fig. 10). These primary tensional faults appear before the initiation of the bounding normal ring-faults which facilitate roof collapse. Since the numerical models used in this and previous papers use elasticity to model the host rock in which the magma chamber is situated, they record only the first instantaneous stress response of the rock to the magma chamber deflation. The question is whether this initial point of maximum tensile stress at surface corresponds to the one related to the formation of the bounding ring faults (within the critical distance of [C3]) as suggested by previous authors (e.g. Gudmundsson, 1998; Folch and Marti, 2004), or not. Contrary to prior interpretations, we suggest that the peak tensional stress recorded at surface by the numerical models is instead related to the position of initial tensional fractures appearing prior to the collapse caldera controlling faults, as seen in analogue experiments.

Therefore while the three critical conditions [C1–C3] for ring fault initiation (see Section 2.2) are in good agreement with rock mechanics principles and evidence from field observations and analogue experiments for the formation and position of the bounding sub-vertical ring-faults, the critical distance defined in [C3] cannot be applied to the results of numerical models implementing elasticity such as those presented here and in previous works (e.g. Gudmundsson, 1998; Folch and Marti, 2004). Satisfaction of conditions [C1] and [C2] is still crucial for the formation of all caldera-related faults or fractures, and results from additional investigations into this are part of a separate communication.

Despite the abovementioned observations, the results of this study are still highly relevant in illustrating how mechanical layering affects the tensional stress-field at the Earth's surface, which has important implications for the initiation of all surface fractures and faults related to caldera collapse.

5. Summary and conclusions

Numerical models looking at the stress-field distribution created by a magma chamber subjected to under-pressure were carried out to investigate the effects of mechanical layering in influencing the initiation of normal faulting required for the generation of caldera collapse. The mechanical properties of seven thin crustal layers placed above the magma chamber were varied in order to generate different stratigraphic configurations. Models simulating a homogeneous host rock were also run as a reference.

Our results indicate that the physical properties of the overlying substrata above a decompressing magma chamber can influence the magnitude, and to a lesser extent the position, of tensional stress occurring at the Earth's surface and thus can encourage or discourage satisfaction of critical conditions required for ring-fault initiation, specifically [C1]: the maximum value of tensional stress must occur at the Earth's surface, and [C3]: the maximum tensional stress at surface must peak approximately above the lateral ends of the magma chamber.

Overall, the addition of mechanically soft layers, such as pyroclastic deposits, will generate greater tensional stress at the surface and this stress is further increased by increasing the thickness of the soft material. Conversely the addition of mechanically stiff layers, such as lavas, will reduce surface tensional stress. Increasing the proportion of soft:stiff layers similarly results in greater tension at surface. For a given proportion of soft to stiff material the vertical order and depth of layers is also shown to be important. A soft layer located at greater depths will increase surface tension, whereas the deeper a stiff layer occurs, the less tension results at the Earth's surface. Regardless of the depth

configuration, a soft layer placed below a stiff layer will produce greater tension at the Earth's surface compared with a homogeneous model, whilst a stiff layer located below a soft layer will always generate less tension at the surface.

The results suggest that volcanic edifices that include layers of contrasting mechanical properties, particularly soft pyroclastic units, are more likely to form the critical stress conditions required for fracture/ring-fault initiation at surface. Edifices composed of predominantly stiff units, such as basaltic shields, are less likely to reach these conditions as also shown by field observations (e.g. Folch and Marti, 2004). Ongoing volcanic activity may act to further affect a volcano's future collapse potential by depositing additional mechanically contrasting layers either at surface by eruption or at depth by intrusion. In this way a volcano over time could achieve a more or less favourable configuration for ring-fault initiation and therefore collapse.

A brief comparison between the results presented here and previous analogue models, suggests that the position of peak tensional stress at surface derived by the numerical models does not represent that related to the position of the bounding ring-fault, but is instead related to the position of initial tensional fractures appearing prior to the collapse faults.

Despite this observation, the results of this study are still highly relevant in illustrating how knowledge of crustal mechanical properties beneath a volcano is therefore vital for assessing the likelihood of future collapse, not least because mechanical layering represents a first-order variable in the rare achievement of ring-fault formation and caldera collapse.

Acknowledgments

The research was supported by NERC (studentship grant NE/F007299/1), the Spanish MEC (grant 2007-0400) and the Royal Society (International Joint Project grant JP071072 and University Research Fellowship UF051396). We wish to thank Agust Gudmundsson and Yan Lavallée for their thoughtful and constructive comments, which led to improvements of this paper.

References

- Acocella, V., Cifelli, F., Funiello, R., 2000. Analogue models of collapse calderas and resurgent domes. *Journal of Volcanology and Geothermal Research* 104 (1–4), 81–96.
- Acocella, V., Cifelli, F., Funiello, R., 2001. Formation of nonintersecting nested calderas: insights from analogue models. *Terra Nova* 13, 58–63.
- Acocella, V., Funiello, R., Marotta, E., Orsi, G., de Vita, S., 2004. The role of extensional structures on experimental calderas and resurgence. *Journal of Volcanology and Geothermal Research* 129 (1–3), 199–217.
- Allen, S.R., 2001. Reconstruction of a major caldera forming eruption from pyroclastic deposit characteristics: Kos Plateau Tuff, eastern Aegean Sea. *Journal of Volcanology and Geothermal Research* 105, 141–162.
- Apra, C.M., Hildebrand, S., Fehler, M., Steck, L., Baldrige, W.S., Roberts, P., Thurber, C.H., Lutter, W.J., 2002. Three-dimensional Kirchhoff migration; imaging of the Jemez volcanic field using teleseismic data. *Journal of Geophysical Research* 107 (B10), 2247. doi:10.1029/2000JB000097.
- Bailey, R.A., Dalrymple, G.B., Lanphere, M.A., 1976. Volcanism, structure, and geochronology of Long Valley Caldera, Mono County, California. *Journal of Geophysical Research* 81 (5), 725–744.
- Bell, F.G., 2000. *Engineering Properties of Rocks*, 4th ed. Blackwell, Oxford. 482 pp.
- Browne, B.L., Gardner, J.E., 2004. The nature and timing of caldera collapse as indicated by accidental lithic fragments from the AD-1000 eruption of Volcán Ceboruco, Mexico. *Journal of Volcanology and Geothermal Research* 130, 93–105.
- Burov, E.B., Guillou-Frottier, L., 1999. Thermomechanical behaviour of large ash flow calderas. *Journal of Geophysical Research* 104 (B10), 23081–23109.
- Codina, R., Folch, A., 2004. A stabilized finite element predictor–corrector scheme for the incompressible Navier–Stokes equations using a nodal based implementation. *International Journal of Numerical Methods in Fluids* 44, 483–503.
- Druitt, T.H., Sparks, R.S.J., 1984. On the formation of calderas during ignimbrite eruptions. *Nature* 310, 679–681.
- Folch, A., Marti, J., 2004. Geometrical and mechanical constraints on the formation of ring-fault calderas. *Earth and Planetary Science Letters* 221 (1–4), 215–225.
- Garcia, M.O., Haskins, E.H., Stolper, E.M., Baker, M., 2007. Stratigraphy of the Hawaii i Scientific Drilling Project core (HSDP2): anatomy of a Hawaiian shield volcano. *Geochemical Geophysical Geosystem* 8, Q02G20. doi:10.1029/2006GC001379.

- Geyer, A., Martí, J., 2008. The new worldwide collapse caldera database (CCDB): a tool for studying and understanding caldera processes. *Journal of Volcanology and Geothermal Research* 175 (3), 334–354.
- Geyer, A., Martí, J., 2009. Stress fields controlling the formation of nested and overlapping calderas: implications for the understanding of caldera unrest. *Journal of Volcanology and Geothermal Research* 181 (3–4), 185–195.
- Geyer, A., Folch, A., Martí, J., 2006. Relationship between caldera collapse and magma chamber withdrawal: an experimental approach. *Journal of Volcanology and Geothermal Research* 157 (4), 375–386.
- Goff, F., 2002. Geothermal potential of Valles Caldera, New Mexico: Ghc bulletin, pp. 7–12. WWW page.
- Goodman, R.E., 1989. *Introduction to Rock Mechanics*, 2nd ed. Wiley, New York. 552 pp.
- Gray, J.P., Monaghan, J.J., 2004. Numerical modelling of stress fields and fracture around magma chambers. *Journal of Volcanology and Geothermal Research* 135, 259–283.
- Gudmundsson, A., 1988a. Formation of collapse calderas. *Geology* 6 (9), 808–810. doi:10.1130/0091-7613(1988)016<0808:FOCC>2.3.CO;2.
- Gudmundsson, A., 1988b. Effect of tensile stress concentration around magma chambers on intrusion and extrusion frequencies. *Journal of Volcanology and Geothermal Research* 35, 179–194.
- Gudmundsson, A., 1998. Formation and development of normal-fault calderas and the initiation of large explosive eruptions. *Bulletin of Volcanology* 60, 160–171.
- Gudmundsson, A., 2006. How local stresses control magma-chamber ruptures, dyke injections, and eruptions in composite volcanoes. *Earth-Science Reviews* 79, 1–31.
- Gudmundsson, A., 2007. Conceptual and numerical models of ring-fault formation. *Journal of Volcanology and Geothermal Research* 164, 142–160.
- Gudmundsson, A., 2009. Toughness and failure of volcanic edifices. *Tectonophysics* 471 (1–2), 27–35.
- Gudmundsson, A., Brenner, S.L., 2005. On the conditions of sheet injections and eruptions in stratovolcanoes. *Bulletin of Volcanology* 67 (2005), 768–782.
- Gudmundsson, A., Philipp, S.L., 2006. How local stress fields prevent volcanic eruptions. *Journal of Volcanology and Geothermal Research* 158, 257–26.
- Gudmundsson, A., Martí, J., Turon, E., 1997. Stress fields generating ring faults in volcanoes. *Geophysical Research Letters* 24, 1559–1562.
- Guillou-Frottier, L., Burov, E.B., Milési, J.-P., 2000. Genetic links between ash-flow calderas and associated ore deposits as revealed by large-scale thermo-mechanical modeling. *Journal of Volcanology and Geothermal Research* 102, 339–361.
- Heiken, G., Goff, F., Gardner, J.N., Baldrige, W.S., 1990. The Valles/Toledo caldera complex, Jemez Volcanic field, New Mexico. *Annual Review of Earth and Planetary Sciences* 18, 27–53.
- Hudson, J.A., Harrison, J.P., 1997. *Engineering Rock Mechanics: An Introduction to the Principles*. Elsevier, Oxford. 444 pp.
- Kavouridis, T., Kuris, D., Leonis, C., Liberopoulou, V., Leontiadis, J., Panichi, C., La Ruffa, G., Caprai, A., 1999. Isotope and chemical studies for a geothermal assessment of the island of Nisyros (Greece). *Geothermics* 28 (2), 219–239.
- Kennedy, B., Stix, J., Vallance, J.W., Lavallée, Y., Longpre, M.-A., 2004. Controls on caldera structure: results from analogue sandbox modeling. *Geological Society of America Bulletin* 116 (5/6), 515–524.
- Komuro, H., 1987. Experiments on cauldron formation: a polygonal cauldron and ring fractures. *Journal of Volcanology and Geothermal Research* 31, 139–149.
- Komuro, H., Fujita, Y., Kodama, K., 1984. Numerical and experimental models on the formation mechanism of collapse basins during the Green Tuff orogenesis of Japan. *Bulletin of Volcanology* 47–3.
- Lavallée, Y., Stix, J., Kennedy, B., Richer, M., Longpre, M.A., 2004. Caldera subsidence in areas of variable topographic relief: results from analogue modeling. *Journal of Volcanology and Geothermal Research* 129 (1–3), 219–236.
- Lavallée, Y., de Silva, S., Salas, G., Byrnes, J., 2006. Explosive volcanism (VEI 6) without caldera formation: insight from Huaynaputina volcano, southern Peru. *Bulletin of Volcanology* 68, 333–348.
- Lindsay, J.M., de Silva, S., Trumbull, R., Emmermann, R., Wemmer, K., 2001. La Pacana caldera N. Chile: a re-evaluation of the stratigraphy and volcanology of one of the world's largest resurgent caldera. *Journal of Volcanology and Geothermal Research* 106, 145–173.
- Lipman, P.W., 1992. Ash-flow calderas as structural controls of ore deposits—recent work and future problems. *U.S. Geological Survey Bulletin* 1212, L1–L12.
- Lipman, P.W., 1997. Subsidence of ash-flow calderas: relation to caldera size and magma-chamber geometry. *Bulletin of Volcanology* 59 (3), 198–218.
- Lipman, P.W., 2000. Calderas. In: Sigurdsson, H. (Ed.), *Encyclopedia of Volcanoes*. Academic Press, San Francisco, USA, pp. 643–662.
- Lipman, P.W., 2007. Incremental assembly and prolonged consolidation of Cordilleran magma chambers: evidence from the Southern Rocky Mountain volcanic field. *Geosphere* 3, 42–70. doi:10.1130/GES00061.1.
- Macedonio, G., Dobran, F., Neri, A., 1994. Erosion processes in volcanic conduits and application to the AD 79 eruption of Vesuvius. *Earth Planetary Science Letters* 121, 137–152.
- Martí, J., Ablay, G.J., Redshaw, L.T., Sparks, R.S.J., 1994. Experimental studies of collapse calderas. *Journal Geological Society London* 151, 919–929.
- Martí, J., Folch, A., Neri, A., Macedonio, G., 2000. Pressure evolution during explosive caldera-forming eruptions. *Earth and Planetary Science Letters* 175 (3–4), 275–287.
- Martí, J., Geyer, A., Folch, A., Gottsmann, J., 2008. Experimental, numerical and geophysical modelling of collapse calderas: a review. In: Gottsmann, J., Martí, J. (Eds.), *Caldera Volcanism: Analysis, Modelling and Response*. Elsevier, pp. 233–284.
- Pinel, V., Jaupart, C., 2005. Caldera formation by magma withdrawal from a reservoir beneath a volcanic edifice. *Earth and Planetary Science Letters* 230, 273–287. doi:10.1016/j.epsl.2004.11.016.
- Roche, O., Druitt, T.H., Merle, O., 2000. Experimental study of caldera formation. *Journal of Geophysical Research* 105 (B1), 395–416.
- Rosi, M., Sbrana, A., 1987. Phlegrean fields. In: *Quaderni de "La Ricerca Scientifica"*, vol. 9. CNR, Roma, p. 114.
- Scandone, R., Acocella, V., 2007. Control of the aspect ratio of the chamber roof on caldera formation during silicic eruptions. *Geophysical Research Letters* 34, L22307. doi:10.1029/2007GL032059.
- Sparks, R.S.J., Francis, P.W., Hamer, R.D., Pankhurst, R.J., O'Callaghan, L.O., Thorpe, R.S., Page, R., 1985. Ignimbrites of the Cerro Galan Caldera, NW Argentina. *Journal of Volcanology and Geothermal Research* 24, 205–248.
- Steck, L.K., Prothero Jr., W.A., 1994. Crustal structure beneath Long Valley caldera from modeling of teleseismic P wave polarizations and Ps converted waves. *Journal of Geophysical Research*, B, Solid Earth and Planets 99 (4), 6881–6898.
- Stix, J., Kobayashi, T., 2008. Magma dynamics and collapse mechanisms during four historic caldera-forming events. *Journal of Geophysical Research* 113, B09205. doi:10.1029/2007JB005073.
- Walter, T.R., Troll, V.R., 2001. Formation of caldera periphery faults: an experimental study. *Bulletin of Volcanology* 63, 191–203.
- Williams, H., 1941. Calderas and their origin. In: *Bulletin of the Department of Geological Sciences*, vol. 25(6). California University Publications, pp. 239–346.